scientific reports

Check for updates

OPEN

City bus seat vibration analysis using 6-axis accelerometer and gyroscope sensors

David Eager, Md Imam Hossain✉, Anna Lidfors Lindqvist & Shilei Zhou

This paper analyses different modes and cycles of seat vibration in city buses by analysing acceleration peak magnitudes and their trends and fluctuations in the time domain. The purpose is to find peak vibration modes that exist in the driving patterns of city buses. Analysing peaks in a time series is essential for many applications specifically in vibration analysis because they represent significant events. Using a 6-axis inertial measurement unit device which has accelerometer and gyroscope sensors data were collected from a number of city buses operating. By applying algorithmic filters the g-force peaks present in different acceleration modes were analysed. The particularity of city bus seat vibration and g-force acceleration levels due to effective acceleration in 3-axes are presented and discussed, namely: longitudinal (forward motion), lateral (side-to-side) and vertical (bounce mode) accelerations. It was found that the bus seat root mean square acceleration magnitude of approximately 0.33 g occurred from the major acceleration cycles during bus running. In longitudinal, lateral and vertical directions, 20% of peak acceleration cycles were above 0.20 g, 0.18 g and 0.27 g respectively. Jerk may be a better indicator of passenger discomfort. The results from this study can provide future reference to research directions into understanding city bus seat vibration levels in longitudinal, lateral and vertical directions and also initiatives to mitigate excess bus seat vibration for the riders.

Keywords Bus seat vibration, Vehicle vibration analysis, G-force, Jerk, Bus running, Transport system comfort, Motion sickness

In urban settings, city buses follow particular driving patterns that contribute to seat vibrations, causing discomfort for passengers and their ability to relax during the ride. This usually includes the bus having several different stops for picking up and dropping off passengers, whilst also following urban area speed restrictions and varying traffic congestion. Factors like speed variation and the vibration components associated with vehicle dynamics, including engine vibration, are also likely to differ[1]. Thus, the dynamics and ride experience of city buses are different from those of coach buses which have far fewer stops. Due to the many stopping and starting points for city buses passengers experience multiple acceleration and deceleration cycles during their ride. The ride experience and quality can be derived from the bus seat g-force acceleration in x, y and z directions which are primarily influenced by the bus driver's driving behaviour and vehicle and road structure dynamics.

The vibration caused by different acceleration cycles is of immense scientific and practical applications like vibration in the elevator (lift). Especially, the acceleration and deceleration cycles presented in increasing the speed from zero, navigating through the route and traffic and decreasing the speed to zero have human vibration response and also economy of operating the vehicle energy efficiently. Objects in motion, such as modes of transportation, have vibration that is different from the vibration of a stationary platform by the very nature of the dynamics and its implication. Vibration amplitude, mode and duration signify vibration response by the receiving system. City buses need to optimise several factors such as reaching different destinations on time, navigating crowded traffic in city areas, providing passengers with a ride experience without significant motion sickness and finally increasing fuel efficiency.

The problem of ride vibration has existed since the earliest forms of transportation and has been given significant attention in research. For instance, the vibrations from trains greatly affect ride comfort and safety, as intense vibrations can result in derailments[2]. Among the various factors that decrease vehicle rider comfort, a main concern is the vibration caused by the movement of vehicles including buses. Specifically, when the movement of the vehicle is not smooth and there is sudden thrust, stopping or rapid change of direction. In engineering practice, factors like road roughness often predominantly influence vehicle vibration responses[1].

Faculty of Engineering and Information Technology, University of Technology Sydney, Sydney 2007, Australia. ✉email: md.i.hossain@alumni.uts.edu.au

Agostinacchio et al. demonstrated that an uneven road surface produces a significant instantaneous dynamic load. While this load does not influence the overall structural response, it does impact the comfort of the ride for passengers[3]. The driving style of different drivers can also affect the riding conditions for passengers, where aggressive, insecure or inexperienced driver may cause a more rapidly changing driving cycle. Analysing longitudinal acceleration trends in typical bus operations aids in pinpointing risky driver conduct, while prolonged data examination allows for evaluating the likelihood of accidents resulting from such behavior[4]. In addition, driving style discrepancies across different road conditions, even among experienced bus drivers was noted to result in variances in fuel consumption[5]. Studies have indicated that each driver interprets the environment uniquely and responds subjectively to varying road conditions, which in response was evident in their acceleration patterns[6,7].

When a vehicle's driving path is not ideal it can cause high jerk or an instantaneous change in the lateral g-force. The path performance of an object in motion can be modelled from highly sensitive factors such as centrifugal jerk and yaw rate as both are related to the radius of curvature of the trajectory[8]. Ideally, the vehicle path would comprise of a continuous curvature path of various clothoid segments that require a minimal amount of veering effort. Clothoid transitions have been used in roller coaster designs for decades to reduce vibration discomfort[9], by reducing the forces and jerk levels imposed upon the body[10].

Förstberg describes variables that influence a rider's comfort including human factors (such as age and gender), environmental factors (such as temperature, noise, and pressure), spatial factors (such as work-space, legroom, seat shape) and dynamic motion factors[11]. Dynamic factors such as vibration and acceleration could introduce motion sickness and posture difficulty for the passengers when limit thresholds are crossed. A mixture of long-term vibration and poor sitting posture may develop chronic musculoskeletal disorders, specifically related to the lumbar spine[12–16]. In a seated posture, just one hour of exposure to vibration might lead to muscle fatigue and make the user prone to back injury[17]. There are different ways to express vibration such as displacement, velocity and acceleration. Of these physical quantities, generally, acceleration is often used as the primary source to determine the severity of human exposure to vibration[18]. In a bus, riders experience vibration that is transferred to the whole body through support platform/s such as the seat and/or the bus floor.

Vibrations can disturb rider ease, reduce the ability to perform certain sedentary activities, and depending on the amplitude, direction, frequency and duration of the vibrations may have an impact on health[19]. One of the most objective measures of ride comfort is the vibration of passengers in different axes. Bus passengers most frequently encounter vertical vibrations[20]. Human sensitivity to vibrations differs based on the direction of the vibration and body parts[21]. Also, a rider's discomfort increases with the exposure time to the vibration[21].

Moon and Yi (2008) found that braking acceleration under 0.2 g provides a safe situation for both driver and passengers, based on human driving test data[22]. Whilst in Bae (2019) it was found that the comfort threshold for longitudinal acceleration is between 0.091 and 0.15 g for public transportation. They considered that passengers in public transport prefer smooth steering, braking and acceleration. Sun (2023) tried to establish a relationship between bus speed and motion dynamics based on the suspension stiffness coefficient ratios[20].

Regarding lateral vibration, a test showed that a peak sinusoidal vibration acceleration limit of 0.2 g was acceptable for the majority of people between the frequencies 5 to 8 Hz for a brief duration of time[23]. Bryce (1966) assumed a reasonable approximation of maximum permissible lateral vibration would be 0.31 g at 1 Hz, 0.2 g at 3 Hz, remaining constant at 0.2 g at 8 Hz, then increasing by 1.0 g at 40 Hz during a constant velocity[23].

In an experiment carried out with vertical vibration, the principal resonance frequency decreases from 5 to 4 Hz for forward head movement and from 6 to 5 Hz for vertical head movement when the magnitude of the vibration rises from 0.04 to 0.12 g root-mean-squared (RMS)[24]. This demonstrates that the resonance frequency of body parts depends on the intensity of the vibration. In sitting positions including sitting erect and relaxed when vertical sinusoidal frequencies were set above 2 Hz at vector accelerations under 1 g maximum body strain occurred between 4 and 6 Hz[25]. Literature shows for road vehicle drivers typical exposure levels were at an RMS acceleration of 0.02 to 0.1 g[26,27].

Previously, researchers have used various techniques such as mathematical modelling and computer simulation to study bus acceleration modes and vibrations correlations to comfort[20,28–31]. For instance, bus driving acceleration modes based on theoretical self-defined road excitations were modelled by formulating differential equations and analytical solutions[20]. However, in this paper bus motion acceleration modes in city driving are experimentally verified and analysed based on g-force acceleration data captured during real-life driving. This is done by identifying peak vibration cycles presented in the city bus seat that may impact passenger comfort using a portable inertial measurement unit (IMU) device. The results show the continuous vibration levels and the sudden forces riders are exposed to by the bus seat during the drive that could disturb their posture or dislodge them from their position. The limit peak values of acceleration cycles as read by the IMU device are presented which can be utilised in defining future research objectives and frameworks.

This paper is organized as follows: Section 2 gives an insight into the process of bus seat vibration data collection setup and IMU data trends observed. In Sect. 3, IMU bus data modelling techniques involved in extracting peak acceleration/deacceleration cycles are described. Sections 4 and 5 analyse the peak acceleration/deacceleration cycles of the bus data and provide an overall statistical overview of the bus peak acceleration/deacceleration results. In Sect. 6, future work relating to the research is pointed out. Conclusions are drawn in Section 7.

Bus seat vibration data collection and processing

Vibration data collection

The seat vibration data was collected from 30 buses driving different routes in a city using an IMU (Yost Lab's proprietary portable 3-Space Data Logger). Despite the growing popularity of installing extensive permanent sensor networks for the continuous dynamic monitoring of major structures using ambient responses, numerous

Parameter	Value
CompassMinTrust	0.06250
AccelMaxTrust	0.00100
CompassMaxTrust	0.00100
RefVectorMode	Auto
GyroOversampleRate	1
AccelOversampleRate	1
CompassOversampleRate	1

Table 1. Yost 3-Space Data Logger configuration.

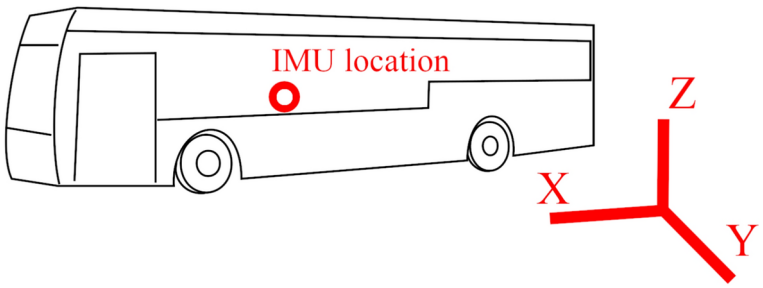

Fig. 1. A city bus diagram and location of IMU device for capturing acceleration and gyroscope data.

constructions can only be monitored intermittently and briefly due to budgetary, technical, and practical limitations[32]. The IMU recorded data via its internal Micro-electromechanical systems (MEMS) accelerometer and gyroscope sensors and is capable of capturing vibration of up to 24 g and ± 2000 °/s respectively. Additionally, the device is equipped with a compass with magnetic induction configured to be 1.3 gauss and uses an onboard Kalman-based orientation algorithm which allows orientation to be relative to an absolute reference. The IMU data logger is equipped with a battery and has a built-in SD card to capture data in a self-contained manner. The sensors on the device were calibrated and configured using Yost Labs 3-Space Sensor Software Suite using auto-calibration function of the software as given in Table 1. The IMU was able to save sensor outputs in its SD card in different formats as defined in the capture.cfg file where corrected sensor data were selected for the bus seat vibration measurement. Thus, the configured corrected accelerometer and gyroscope sensors acceleration and angular velocity data were saved in the SD card in g and rad/s units respectively.

Using the IMU device the bus seat vibration data was gathered from various city buses operating on different routes within the same city. To maintain consistent data capture, the IMU was located in a common location in all test vehicles as displayed in Fig. 1. Figure 1 contains a diagram of a city bus where the red dot shows the approximate location of the bus seat for the IMU device placement for acceleration measurement and data capture. The orientation of the Cartesian coordinate system used is also defined. The X, Y and Z-axes measured the longitudinal, lateral and vertical accelerations respectively. The sensors had their axis aligned to the bus heading direction so that the longitudinal, lateral and vertical acceleration of the bus was captured by respective sensor axes for the most part. Figure 2 shows a diagram of the IMU device placement on the passenger seat inside the bus.

The IMU device has different modes of operation for sampling rate versus data capture accuracy. Zini's study demonstrates that merely increasing the sample size does not lead to result convergence, indicating that the vibration's characteristics inherently affect the damping values[33]. Experimentation with different modes on the bus seat established that 75 samples per second was sufficient for data capturing as this had a good signal-to-noise ratio. This correlates with the ideal sampling rate derived by the IMU sensor's built-in smart motion detection algorithm. There were minimal amplitudes of higher frequency vibrations observed in the bus seat measurements. The data capture duration for the different busses was between 6 and 22 minutes, and the speed never exceeded 50 kph.

Vibration data processing

Figure 3 depicts the process of bus seat vibration data analysis. After capturing the bus seat vibration data using the IMU device, data were cleaned up by discarding bus stationary points data and data that were affected by excessive sensors drifting. Hence, tha data captured for the 30 different seat vibration acceleration is presented where buses were always moving. To better understand the global features from the sensors' outputs, a 400 s window and −1 to +1 g amplitude scope was used for overall acceleration features analysis. A close observation of the global data from all bus data established the requirements for designing algorithmic filter window sizes for the accelerometer data. Multiple algorithmic filters were used for the acceleration data where each filter was primarily tweaked for analysing and detecting a particular peak acceleration mode and pattern in the accelerometer data. By using gradient and envelope peak detection algorithms, the peak points of interest in the

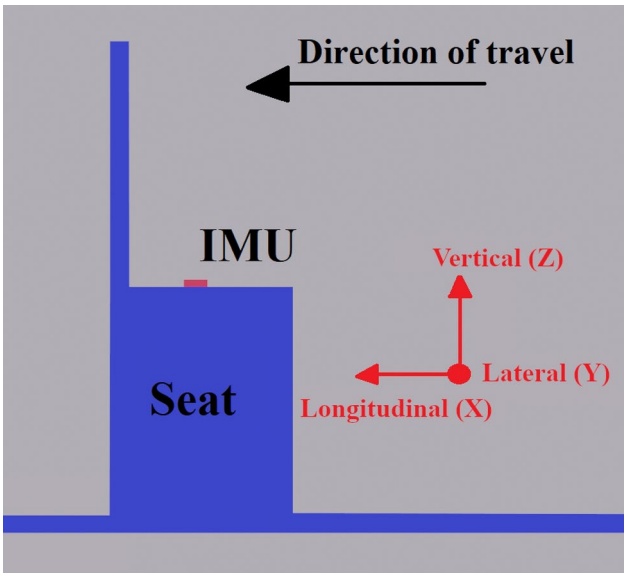

Fig. 2. Placement of the IMU on the bus passenger seat and IMU axis directions relative to bus travel direction.

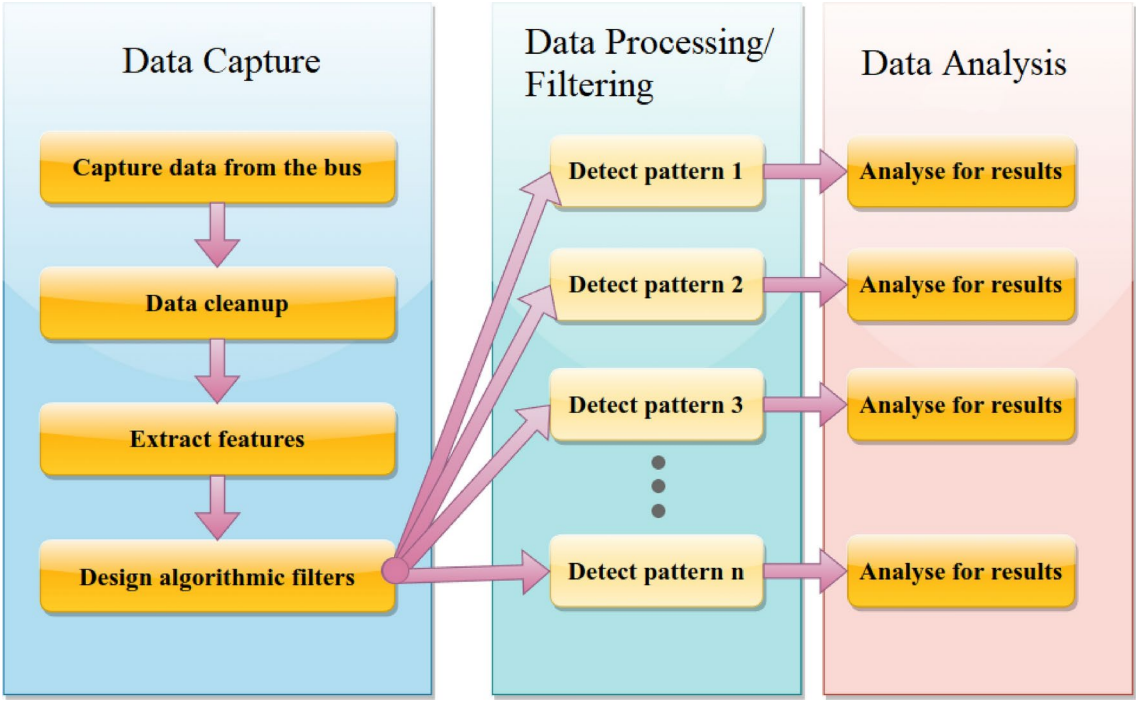

Fig. 3. Process of bus seat vibration data analysis.

acceleration data were extracted for results analysis. It should be noted that different peak detection algorithms derived different acceleration types and corresponding magnitudes from the data as explained in Section 3.

After cleaning the captured acceleration data, it was corrected for pattern finding and recognition using peaks and envelope detection methods. Below are the major steps taken for performing corrective actions on the acceleration data before analysing acceleration.

Analysis of the power spectrum of the accelerometer data indicated that the major acceleration modes for the bus seat were low-frequency accelerations. Figure 4 presents the frequency analysis of a bus trip where major acceleration frequencies are shown for the horizontal plane of the bus (longitudinal and lateral motion). The spectrum displays frequencies derived from acceleration data recorded throughout the entire bus running duration, encompassing both transient and steady-state events. As can be seen from the plot, with the increasing

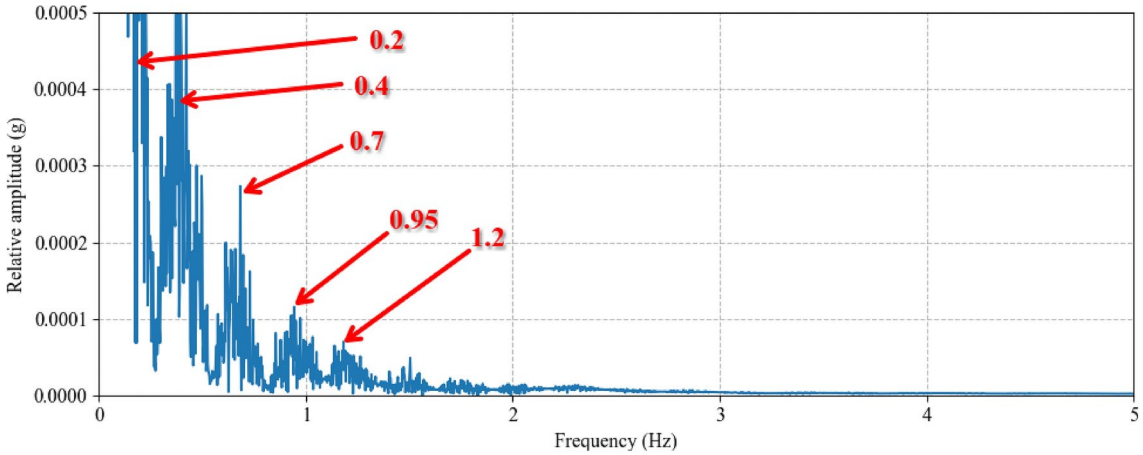

Fig. 4. Power spectrum of a bus trip for horizontal plane accelerations (longitudinal and lateral combined) of the bus seat.

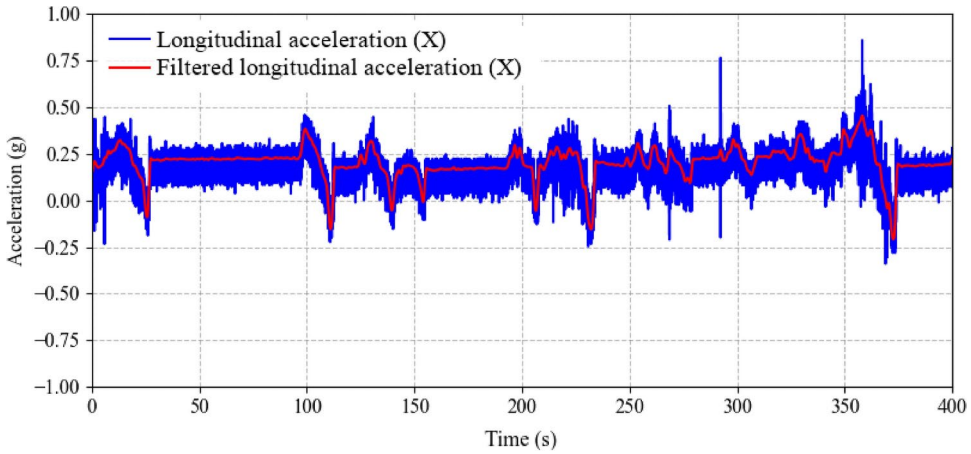

Fig. 5. Envelope algorithmic filter result showing limit continuous longitudinal acceleration used for finding acceleration patterns and modes.

frequency of the acceleration, the amplitude decreases for the bus running where peak frequencies are 0.2, 0.4, 0.7, 0.95 and 1.2 Hz. Lower peak frequencies, such as 0.4 Hz and 0.2 Hz, can be attributed to the general motion of the bus, including steady-state driving forces and thrust cycles. These frequencies are of particular interest in this case due to their higher amplitudes.

A custom envelope approximate filter based on a moving standard deviation and moving average filters was used for producing the approximate continuous limit acceleration while removing high-frequency noise from the accelerometer data. The envelope acceleration is more sensitive to brief, high-frequency impulses than RMS acceleration where the city bus acceleration could be unpredictable due to traffic avoidance. Also, envelope analysis is superior to traditional raw vibration signal analysis when it comes to fault detection[34]. The purpose of employing moving averages or moving-average envelopes is to detect shifts in trends[35]. As this acceleration is also closely related to the RMS acceleration of the vibration acceleration cycle peaks, the longitudinal and lateral acceleration modes were synthesised from this acceleration. This is a two-step process: firstly, a moving average filter of optimised window size cancels out high frequencies (higher than 100 Hz) from the captured low sampling rate data. This is an essential step as a Fast Fourier Transform (FFT) based high frequencies (higher than 75 Hz) de-noising filter would not work with low sampling rate data as captured for the bus seat acceleration data. In the second step, the moving standard deviation was convoluted to the moving average acceleration data by adding two values together resulting in envelope acceleration. Figure 5 shows filtered longitudinal acceleration based on the envelope approximate filter method. The results produced by this method were used for finding longitudinal and lateral acceleration cycle peaks and modes.

Figure 6 illustrates the longitudinal and vertical acceleration of a bus running for a 200 s duration. The 200 s acceleration window shows both the acceleration and deceleration phases of the bus running. It shows the characteristic differences between longitudinal and vertical acceleration. Vertical acceleration was attributed to the bus suspension bouncing during the accelerating and braking phases. The acceleration profile suggests

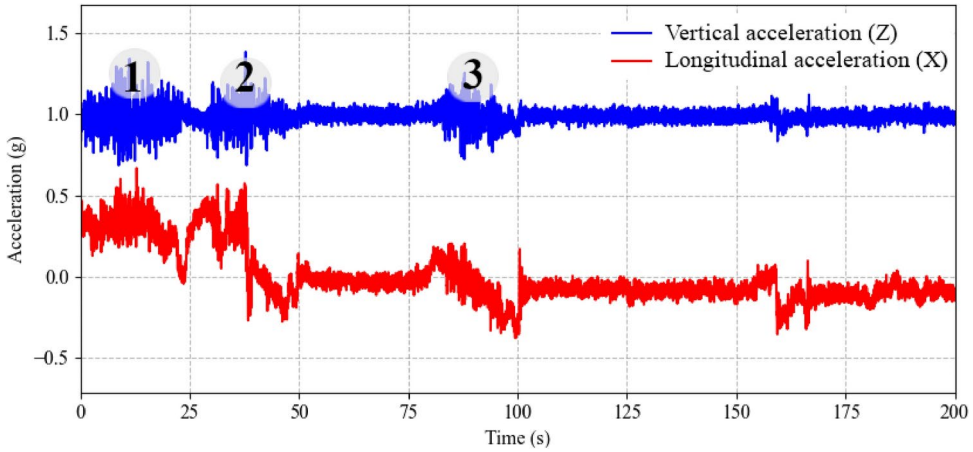

Fig. 6. Longitudinal and vertical accelerations of a bus running.

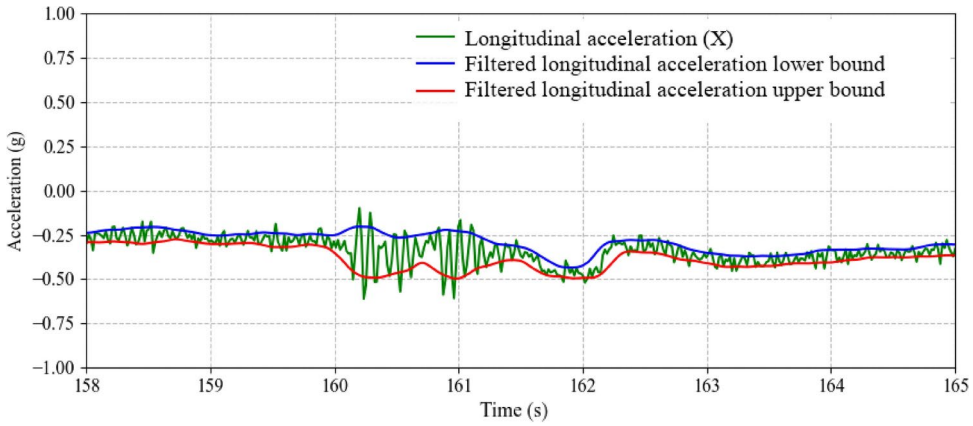

Fig. 7. Longitudinal acceleration of a bus during the sudden brake.

that the vibration is a Morlet Wavelet function in nature where acceleration fluctuates around the peak value. The amplitude of the vertical acceleration can be found from the envelope accelerations capturing overall acceleration. The difference between the upper and lower bounds of the envelope filter indicates the actual vertical acceleration magnitude. In Fig. 6, labels 1, 2 and 3 indicate the major vertical accelerations. For instance, the first acceleration and deceleration were at the beginning and around 32 s respectively as can be seen from the longitudinal acceleration.

During the analysis it was found that the sudden brakes of the bus also have similar characteristics to the vertical acceleration for the longitudinal acceleration as can be seen from Fig. 7 green plot. As evident, the two vibrations at around 160.3 and 161.0 s caused by a sudden brake have an approximate maximum magnitude of 0.28 g as determined from the difference between upper and lower bounds. Sudden brakes have a vibration acceleration form resembling a Morlet wavelet function. An envelope algorithmic filter was used to find the negative upper bound (red plot) and the negative lower bound (blue plot) of the vibration acceleration.

Figure 8 shows a bus trip steady state acceleration where the speed of the bus remains unchanged. By analysing bus steady state acceleration data, it was found that the bus longitudinal acceleration with constant speed was approximately between −0.135 and +0.05 g as can be seen from Fig. 8, where it is showing acceleration magnitude to be approaching 0.1 g as shown by the orange plot. A lower level of vibration was also observed in the accelerometer sensor where acceleration fluctuated between −0.125 and +0.05 g. This lower acceleration indicates a similar behaviour to when the bus is stationary.

Sensor drifting occurred during data capturing using the IMU device for both the accelerometer and gyroscope data. Figure 9 shows that the gyroscope data has a constant negative drifting gradient over an 800 s running period. Gyroscopes experience bias instabilities where their initial zero reading drifts over time due to the integration of inherent imperfections and noise within the device[36]. The drift in gyroscopes primarily results from the combination of two components: a slowly varying, near-DC variable known as bias instability, and a higher-frequency noise component termed angular random walk (ARW)[36]. Also, it could be found that the dynamic nature of the bus motion path causes this drift (such as roads are not perfectly straight where there is always a turning radius, i.e. a straight path can be considered a path with a 500 m radius even a 1000 m radius).

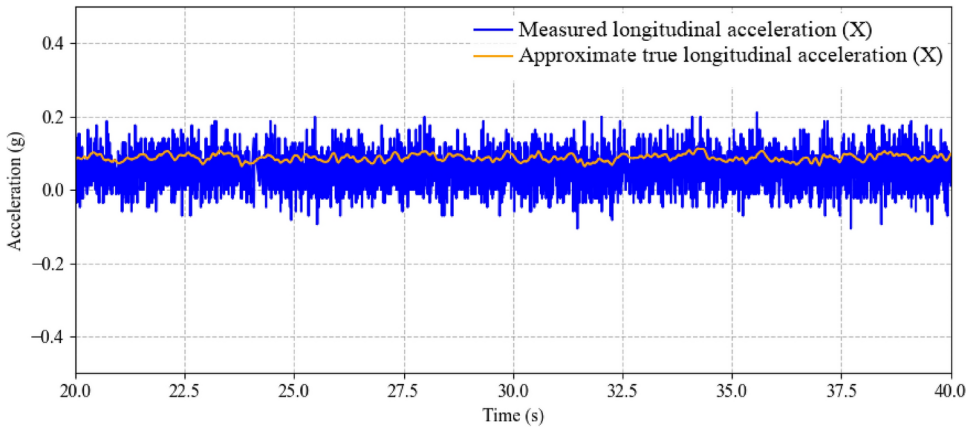

Fig. 8. Steady state bus running condition longitudinal acceleration of the bus.

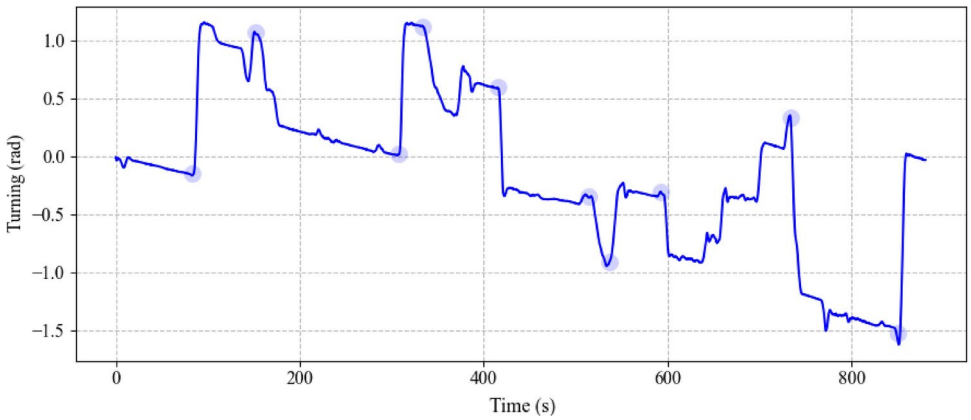

Fig. 9. Gyroscope drifting in the bus turning calculation.

One way to ignore the drift in IMU data is to avoid absolute value, and to take the difference between the peaks and valleys for the acceleration data. Sensor measurement drifting comes from the constant background noise or unwanted vibration presumably relating to bus engine vibrations. Therefore, major acceleration cycles were found by calculating the difference between the consecutive peaks and valleys in the data which did not change regardless of the sensor drifting. Figure 9 shows drifting can be visible throughout the data where turning is constantly reduced at a constant rate. The onset of sharp changes (blue circles) in the bus turning can be seen first at around 90 s where a greater than 60 degrees bus heading change occurred.

For drifting corrections, sensor data captures that created variable drifting over time were discarded, and captures with minimal variation in drifting were used for the acceleration data analysis after applying baseline corrective measures. Baseline correction is necessary when utilising an inconsistent acceleration signal in dynamic analyses[37]. For the gyroscope, it was a near-constant gradient drift with the time while for the accelerometer it was either a near-constant offset from the zero acceleration baseline with every major vibration, movement or a variable gradient descent of the data. The offset for the acceleration was found by finding the bus stationary data point value and convoluting that value with the rest of the data where drifting was occurring. Translating all the data on the acceleration amplitude axis based on global maximum positive and negative accelerations since drifting cannot occur in the global peak to valley/valley to peak occurring in a short period of time. The global peak accelerations provided the offsets necessary for the data translation operations. For instance, in the translation operation when the global maximum and minimum in the acceleration data are respectively $+0.25$ and -0.4 g. The $+0.25$ g offset is added to the acceleration data points as -0.4 g is outside of the absolute maximum acceleration threshold as found from analysing the data. Figure 10 illustrates drifting correction based on the baseline correction method and applying the above-mentioned techniques for acceleration data analysis. The window size for the baseline (blue plot) was calculated using Eq.(1), where a smoothing factor of 10 was deemed to be ideal. The red plot shows drifting corrected data from the original signal (green plot). The filters used the peaks in the data (red circle) to find variable drifting amounts in the data.

$$Window\ size = (Sampling\ rate * 0.02) * Smoothing\ factor \tag{1}$$

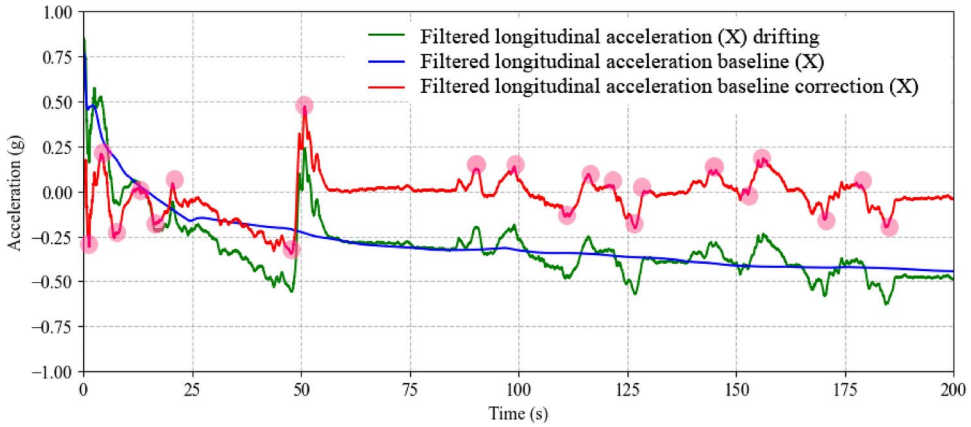

Fig. 10. Longitudinal acceleration data drifting versus drifting corrected longitudinal acceleration.

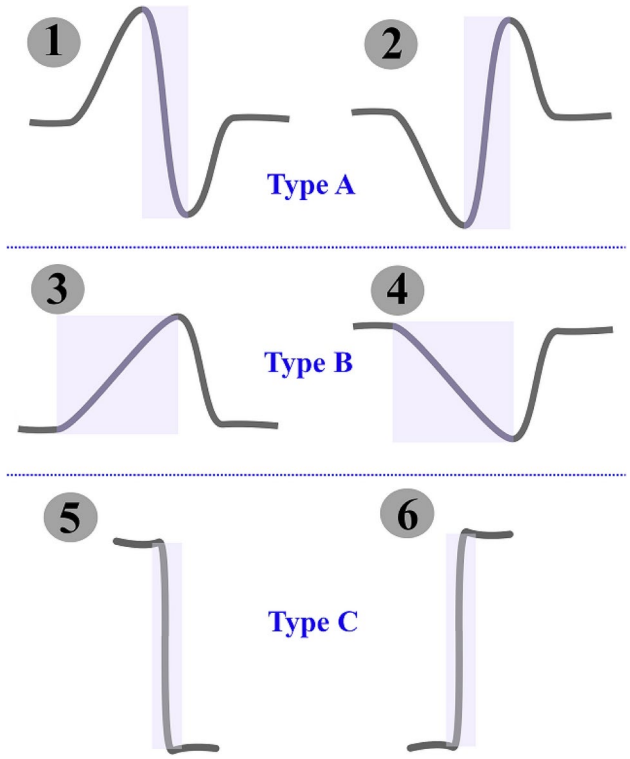

Fig. 11. Major distinguishable acceleration versus time and patterns recognition regions for bus motion transitions.

Modelling of bus seat vibration patterns

Due to the dynamic nature of different peak cycles in a bus trip, and the variability of bus driving modes over an entire bus running period, calculating the RMS for an entire bus running would not show individual details of seat vibrations. Instead, different acceleration cycles and corresponding peak accelerations were modelled and extracted from the filtered acceleration data. Analysing these acceleration cycles provided details about bus seat vibration. In addition, the RMS value of all acceleration cycles provided general acceleration feedback of the bus seat. Below are details about acceleration cycle types and how they were extracted and modelled from the filtered acceleration data.

Different acceleration patterns existing in the longitudinal and lateral acceleration modes were analysed using different algorithmic filters. The major acceleration types can be described as: (i) bus accelerating followed by stopping, (ii) bus stopping followed by accelerating and (iii) just accelerating and decelerating. The first type can be approximated by a first-order Gaussian wavelet while the second type can be approximated by a fractional order Gaussian wavelet. Figure 11 shows the types that exist in the acceleration modes for the bus and the corresponding detection range as shown by the shaded box. Indicated in the image as number 1 in Fig. 11

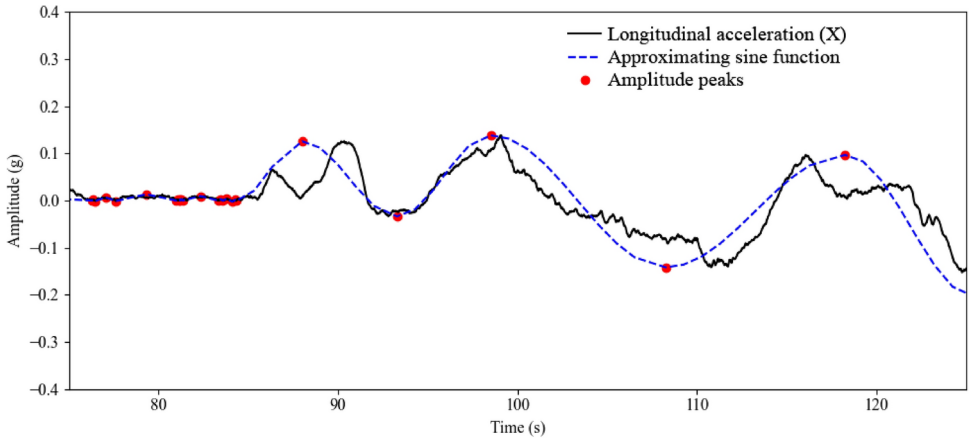

Fig. 12. Acceleration high to low and low to high patterns detection using baseline peaks finding algorithm.

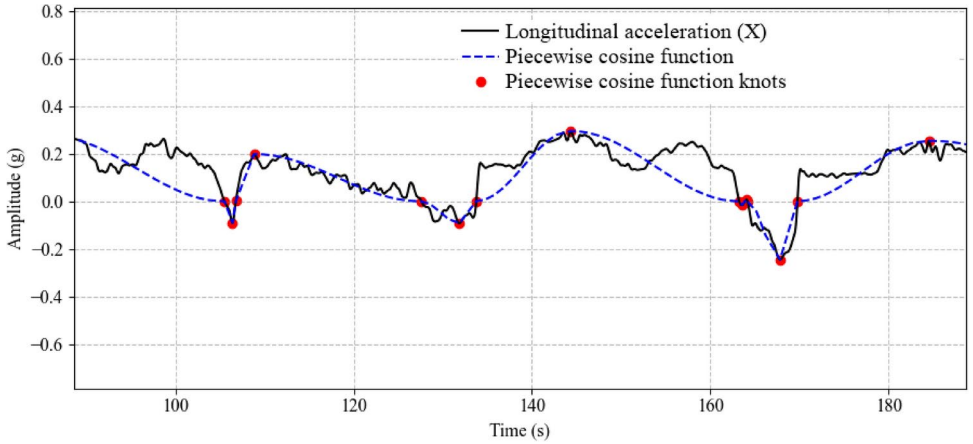

Fig. 13. Acceleration and deceleration patterns detection using baseline peaks finding algorithm.

denotes moderate acceleration followed by braking. The number 2 is moderate braking followed by acceleration. The number 3 is gradual acceleration followed by moderate braking. The number 4 is gradual braking followed by moderate acceleration. The numbers 5 and 6 are sudden stop (−jerk) and sudden start (+jerk) respectively. It can be seen that, in the first and second types, numbers 1 and 2 images in Fig. 11 the change of overall acceleration amplitude (shaded region) is higher than in the number 3 and 4 types. Hence, it is expected that the first and second acceleration types have maximum g-force compared to the third and fourth types. The fifth and sixth types of acceleration occurred in a unpredictable manner where overall g-force shifts to a lower or higher magnitude producing sharp acceleration in a short period of time.

To detect the first and second acceleration types, filtered acceleration data was convoluted such that the baseline (0 amplitude) of the overall data separates the data set into positive (peaks) and negative (valleys). As shown in Fig. 12, the longitudinal acceleration data shows peaks and valleys after the convolution operation on the filtered acceleration data. An approximating sine function was also used for verifying fluctuations of overall acceleration after the convolution operation.

To recognise the third and fourth acceleration types, the convolution operation was followed by a piecewise cosine function where each cosine segment was representative of either the third or fourth acceleration types. As shown in Fig. 13, longitudinal acceleration was divided into piecewise cosine function segments where covariance and correlation values of the segments were used for detecting third and fourth acceleration types.

In addition to the two major acceleration types Type A and B, there were also jerk[38,39] inflection points which are depicted as the fifth and sixth acceleration types in Fig. 11 where the acceleration change is rapid and unpredictable. These additional acceleration types were found by applying a gradient picking algorithm to the filtered acceleration data. The gradient picking algorithm detected the peaks by analysing changes in the slope (gradient) of the signal where a peak is typically characterised by a positive gradient followed by a negative gradient or vice versa. Adjusting of parameters such as threshold values for slope changes was identified from an iterative process where ideal values were found for detecting major peaks in the acceleration signal. Moreover, the gradient picking algorithm found the peaks where the acceleration cycle period is under 3 s. As can be seen

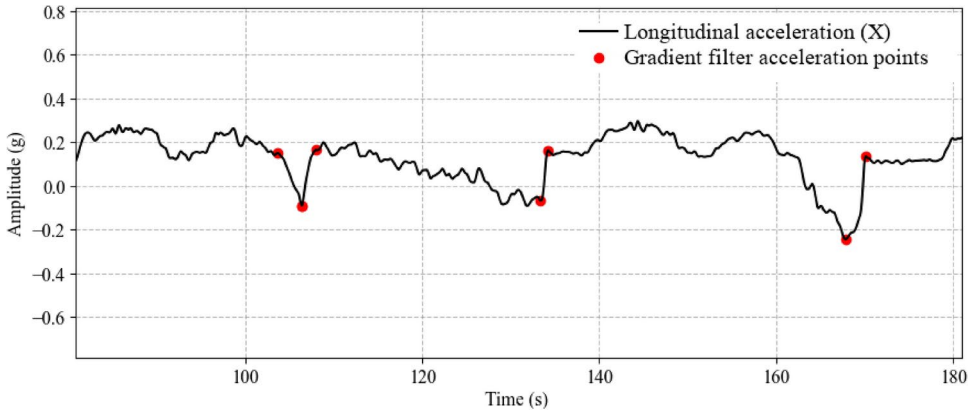

Fig. 14. Detection of sharp acceleration and deceleration change patterns using the gradient picking algorithm.

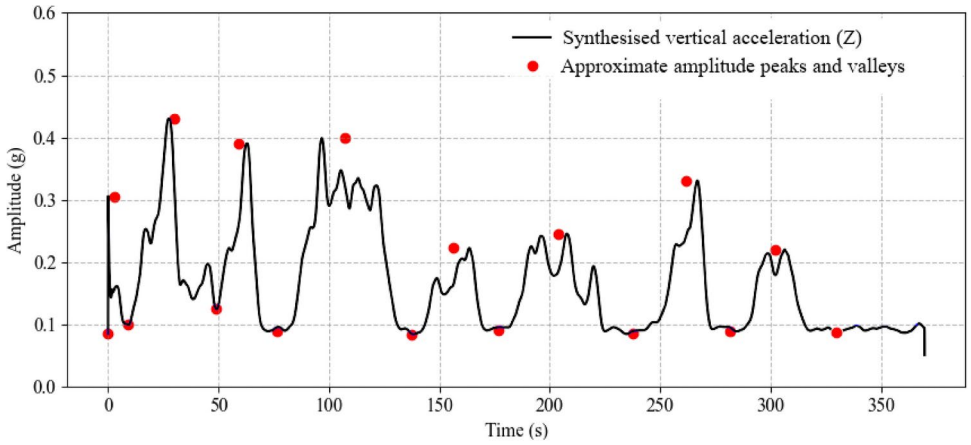

Fig. 15. Bus vertical acceleration data and corresponding peak amplitudes.

from Fig. 14, four high jerk points were found by the gradient picking algorithm within this acceleration data set window.

For vertical acceleration, an envelope analysis was carried out using an envelope algorithmic filter generated synthesised acceleration cycles by calculating the difference between the upper and lower envelopes of acceleration. Originally, envelope analysis could not accurately measure acceleration from mechanical impacts, but since the 1990s, advances in impact peak detection technology have resolved this issue[40]. The resultant difference signal illustrates the variations in the amplitude range of the original signal over time. In the bus stationary conditions, the vertical acceleration value is 1 g where the envelope filter found the variations from this value. The overall process is subtracting the lower envelope from the upper envelope or vice versa depending on which is higher in magnitude and finally subtracting 1 g from the difference value. Figure 15 shows the outcome of this process for vertical acceleration cycles from a bus running. Finally, the peak detection algorithm found the expected peaks and valleys of this signal which were used for finding acceleration cycle duration and amplitude.

Bus seat vibration results

The results from the acceleration cycles and corresponding peaks relating to maximum g-force acceleration (g_{max}) can be divided into three types as depicted in Fig. 11, where the first and second acceleration patterns fall into Type A, the third and fourth acceleration patterns into Type B, and the fifth and sixth acceleration patterns fall into Type C where it is applicable. For longitudinal and lateral accelerations, the results of the seat vibration from bus running are analysed from the perspectives of acceleration ranges, acceleration smoothness and acceleration frequency sections. All the peak acceleration cycles containing their g_{max} and cycle duration are analysed in the acceleration ranges section. The profiles of the peak acceleration cycles are analysed in the acceleration smoothness section. For vertical acceleration, the results of the seat vibration from the bus running show g_{max} and cycle duration of peak acceleration cycles. The profile of the vertical acceleration is mainly of a singular type where the g_{max} and cycle duration determined the vertical acceleration outcome.

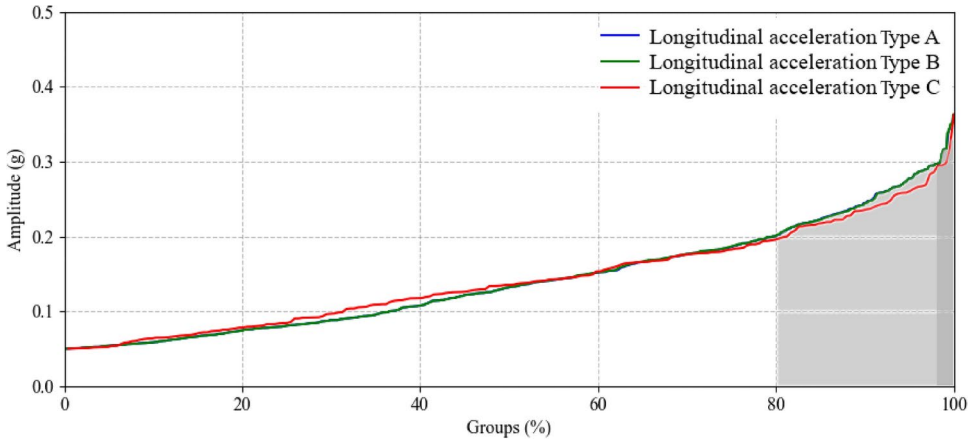

Fig. 16. Bus longitudinal peak acceleration cycles instances ordered from low to high amplitude.

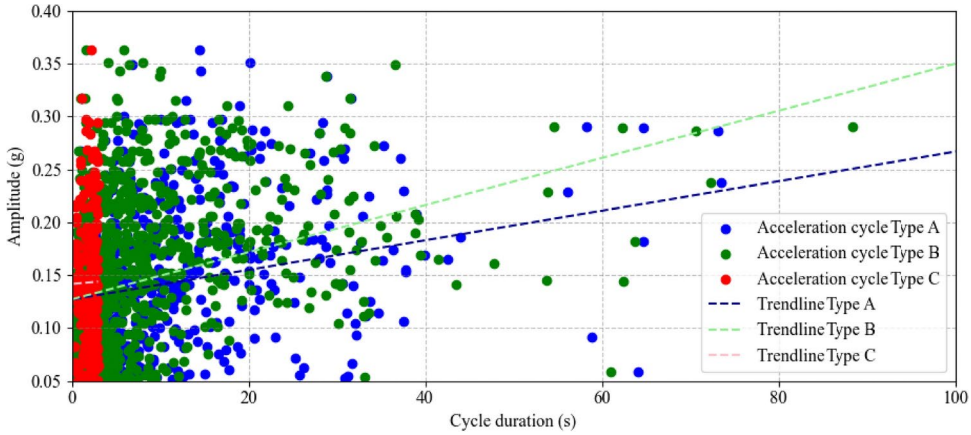

Fig. 17. Bus longitudinal acceleration instance points' peak amplitude versus corresponding cycle duration.

With the acceleration ranges the level of shocks and thrusts in different directions in the seat were analysed. These acceleration modes appear and disappear with a significant change in the speed of the bus and usually occur multiple times during a bus running. The RMS acceleration magnitude was approximately 0.33 g for all longitudinal, lateral and vertical peak acceleration cycles combined. During a bus running, the bus had to increase and decrease speed to move from one stop to the next. The bus had to reduce speed due to traffic, intersection signals and to pick up passengers. On average, there was one period of either increase or decrease of speed of several seconds (accelerating and decelerating) for every 28 to 42 s. This would indicate that throughout a trip a passenger is likely to experience some level of discomfort since the magnitude of acceleration is more than double what was considered a comfortable experience according to research by Bae[41].

The details of the results for longitudinal, lateral and vertical bus seat vibration peak acceleration cycles are given in the following sections.

Longitudinal acceleration analysis

Acceleration ranges

As can be seen from Fig. 16, 50% of the acceleration peaks have g_{max} lower than 0.135 g. This also means 50% of the acceleration peaks have g_{max} greater than 0.135 g. On the other hand, 20% of the acceleration peaks have g_{max} greater than 0.2 g (grey shade). Only 0.9% of the acceleration peaks have g_{max} greater than 0.3 g (dark grey shade).

The histogram data of peak acceleration cycles can be divided into two sections based on the gradient change at 83%. During a bus running, either bus driving acceleration (83% of the time) or bus starting to move and stopping acceleration (17% of the time) could occur. Now, it can be seen that the driving acceleration range was between 0.05 and 0.21 g with the median at 0.12 g. The bus starting to move and stopping acceleration range was between 0.21 g and 0.36 g with the median at 0.25 g from the peak acceleration cycles.

As can be seen from Fig. 17, the majority of the peak acceleration cycles fell under 18, 13 and 2 s cycle duration where the median cycle duration for peak acceleration cycles were 6.3, 3.2 and 2.0 s for Types A, B

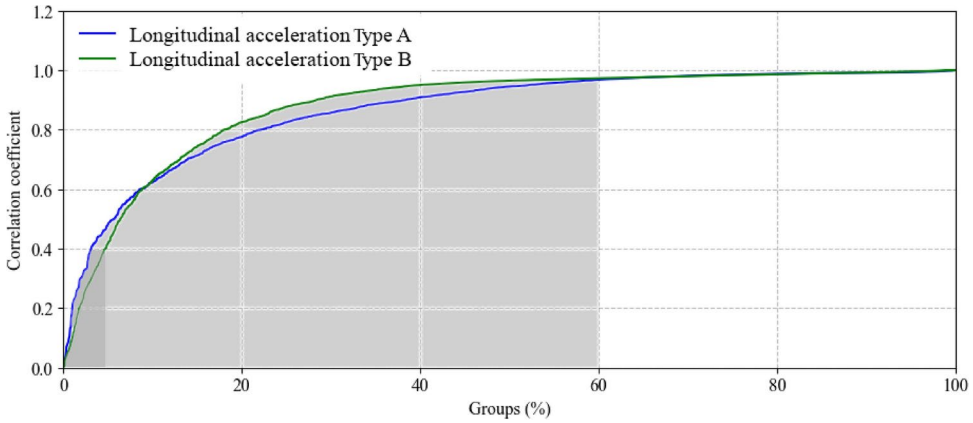

Fig. 18. Bus longitudinal acceleration linearity.

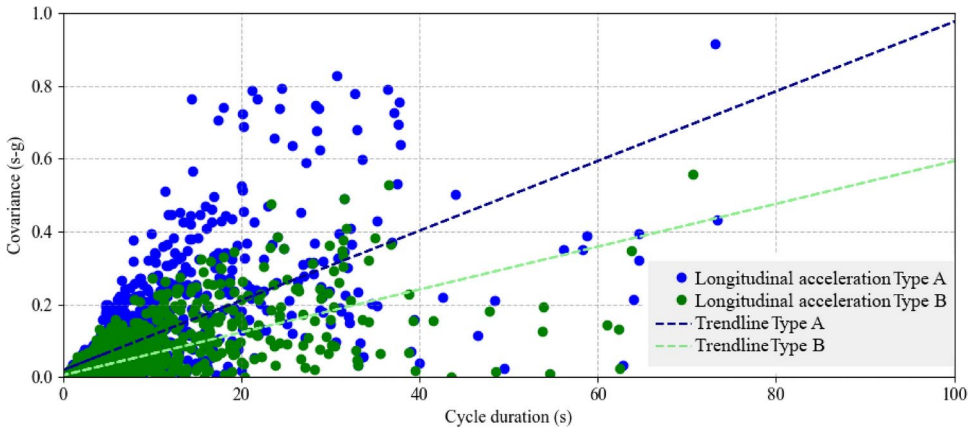

Fig. 19. Bus longitudinal acceleration intensity.

and C respectively. The RMS acceleration of peak cycles was approximately 0.16 g for all Types A, B and C acceleration types.

Acceleration smoothness

Figure 18 depicts the correlation coefficient of peak acceleration cycles for Types A and B acceleration types. The correlation coefficient of the peak acceleration cycles measured linearity and variability in the acceleration types. A streamlined acceleration where acceleration gradually increased or decreased to the peak in a peak acceleration cycle would have a correlation coefficient approaching 1.0. On the other hand, a lower value than 1.0 would indicate there are abrupt fluctuations in the peak acceleration cycle. As can be seen from the plot 60% of the Types A and B peak acceleration cycles have non-linearity or abrupt changes towards the peak acceleration (grey shade) while less than 5% of the peak acceleration cycles have correlation coefficients under 0.4 indicating high fluctuations (dark grey shade). 90% of Type B accelerations showed a more streamlined acceleration phase compared to Type A due to a higher correlation coefficient.

For the Type C peak acceleration, the profile of the peak acceleration cycles is predominantly either an increasing or decreasing acceleration trend without any fluctuations. Thus, it is evident that the correlation coefficient of this type of acceleration cycle would be approaching 1.0.

Figure 19 depicts the covariance of peak acceleration cycles for Types A and B accelerations. Covariance analysis was carried out to find the difference between Types A and B amplitudes in relation to their cycle duration. This can be seen from the trend lines of covariance where Type A had a greater gradient, and thus it played a more dominant role in increasing acceleration with respect to time compared to Type B.

Acceleration frequency

Figure 20 depicts the frequency spectrum of a bus trip showing dominant frequencies exist in the longitudinal acceleration. It can be seen that at lower peak frequencies the amplitude of the acceleration was higher than at the higher frequencies. The relationship between frequency and amplitude is an exponential decay function. The highest longitudinal frequency was at 1.2 Hz and had approximately a relative amplitude of 0.000085 g which translated to 0.085 g from data observation. Also, all the peak frequencies 0.16, 0.4, 0.7, 0.96 and 1.2 Hz had

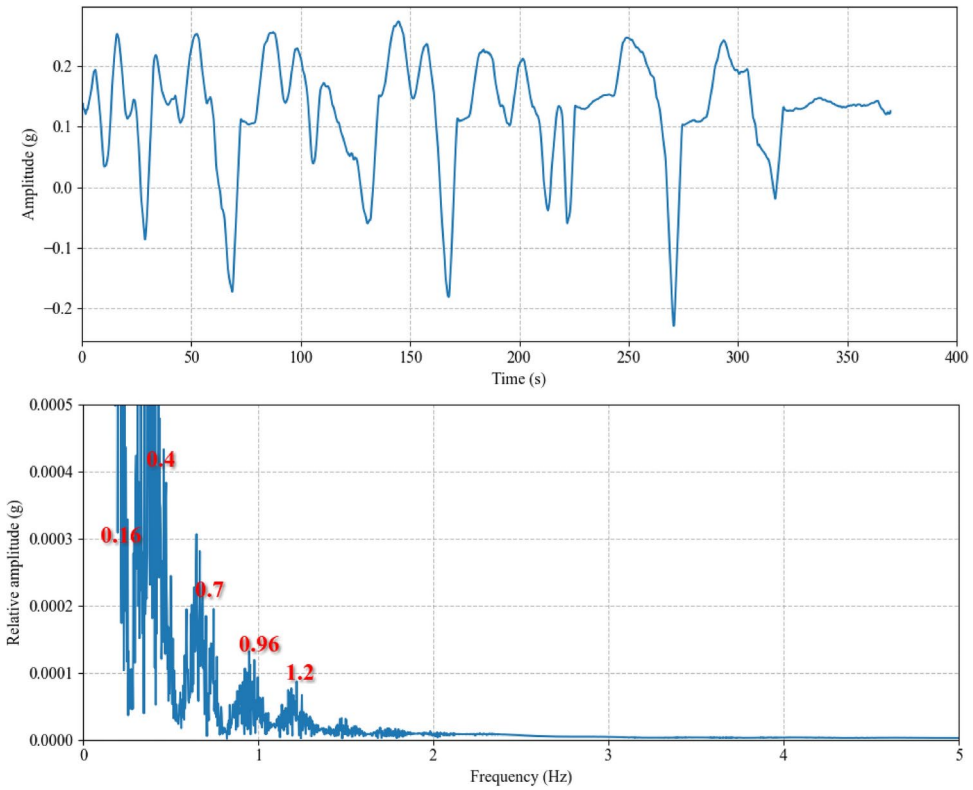

Fig. 20. Power spectrum of a bus running for the longitudinal acceleration of the bus seat showing dominant frequencies.

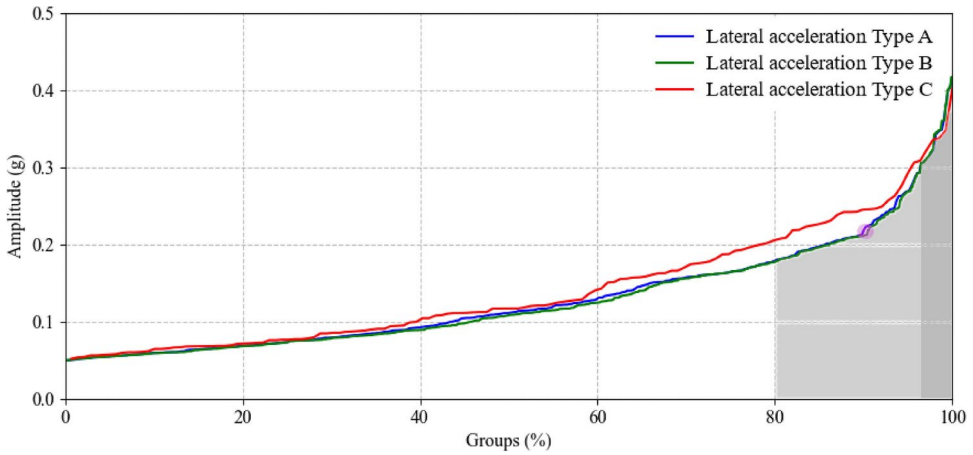

Fig. 21. Bus lateral peak acceleration cycles instances ordered from low to high amplitude.

different amplitudes. This shows that frequencies of the longitudinal seat vibration can be predicted from the longitudinal vibration amplitudes.

From the frequency spectrum, the major acceleration modes can be identified. Peak frequencies 0.7, 0.96 and 1.2 Hz correspond to bus different transient acceleration modes where 0.16 and 0.4 Hz accelerations correlate to gradual bus acceleration modes. The bus was mostly rigid body vibration for the seat vibration where higher frequencies than 1.2 Hz were related to the vibration of the loose parts and could not be found in the frequency spectrum.

Lateral acceleration analysis

Acceleration ranges

As can be seen from Fig. 21, 50% of the acceleration peaks have g_{max} lower than 0.107 g. This also means 50% of the acceleration peaks have g_{max} greater than 0.107 g. On the other hand, 20% of the acceleration peaks have

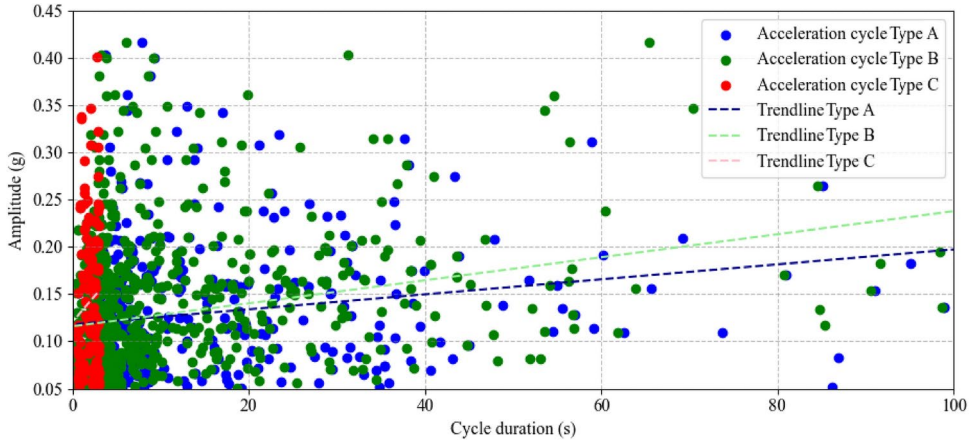

Fig. 22. Peak amplitude of the bus lateral acceleration instance points versus corresponding cycle duration.

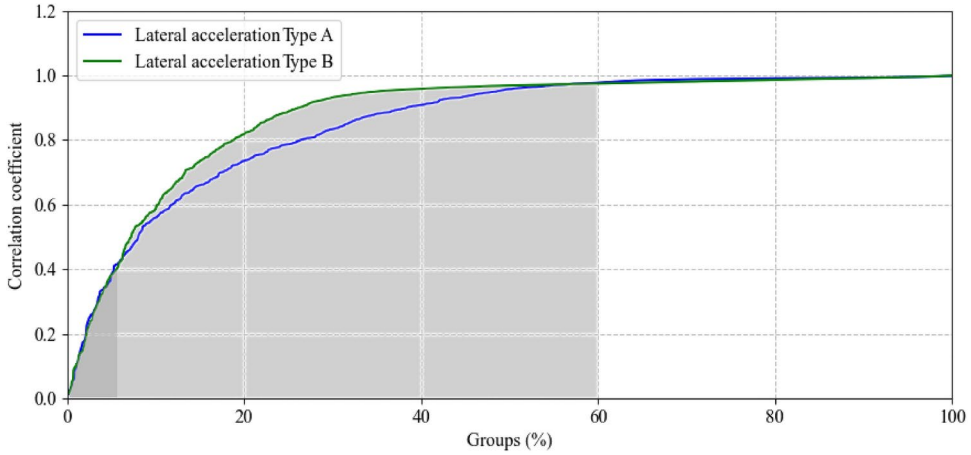

Fig. 23. Bus lateral acceleration linearity.

g_{max} greater than 0.181 g for Type A and Type B (grey shade). Only about 4.3% of the acceleration peaks have g_{max} greater than 0.3 g for Types A and B (dark grey shade area).

The histogram data of peak acceleration cycles can be divided into two sections based on the gradient change at 90.5% (purple circle). During a bus trip, either bus driving acceleration (90.5% of the time) or bus starting to move and stopping acceleration (9.5% of the time) could occur. It can be seen that the driving acceleration range was between 0.05 and 0.25 g with the median at 0.11 g. The bus starting to move and stopping acceleration range was between 0.25 g and 0.42 g with the median at 0.28 g.

Compared to the longitudinal acceleration range the intensity of the g_{max} acceleration range for lateral acceleration was higher during the bus starting to move and stopping.

As can be seen from Fig. 22, the majority of the peak acceleration cycles fall under 24, 19 and 2 s cycle duration where the median duration for peak acceleration cycles were 7.0, 3.4 and 2.0 s for Types A, B and C respectively. The RMS acceleration of peak cycles was approximately 0.15 g for all Types A and B acceleration types respectively. The RMS acceleration for Type C was approximately 0.16 g.

Acceleration smoothness

Figure 23 depicts the correlation coefficient of peak acceleration cycles for Types A and B acceleration types. As can be seen from the plot 60% of the Types A and B peak acceleration cycles had non-linearity or abrupt changes toward the peak acceleration (grey shade) while less than 5.7% of the peak acceleration cycles had a correlation coefficient under 0.4 indicating high fluctuations (dark grey shade). 90% of Type B peak acceleration cycles showed a more streamlined acceleration phase compared to Type A due to a higher correlation coefficient.

For the Type C peak acceleration cycle, the profile of the acceleration cycles was predominantly either an increasing or decreasing acceleration trend without any fluctuations. Thus, it is evident that the correlation coefficient of this type of acceleration cycle would be approaching 1.0 g.

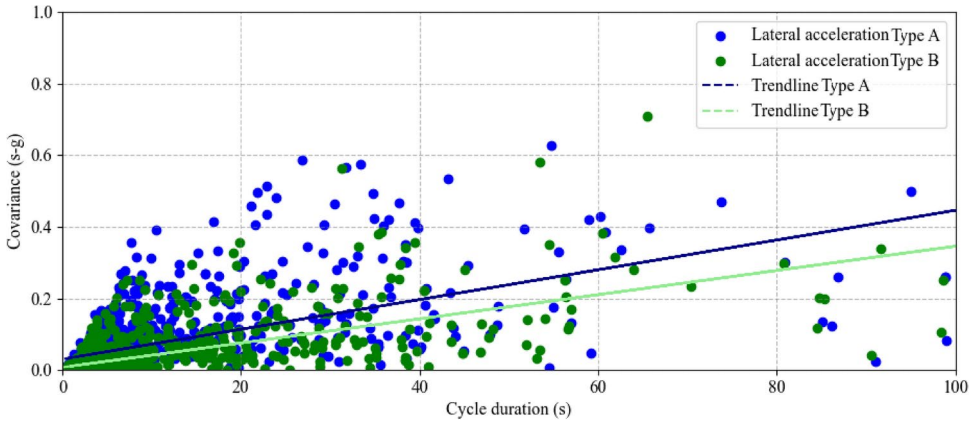

Fig. 24. Bus lateral acceleration intensity.

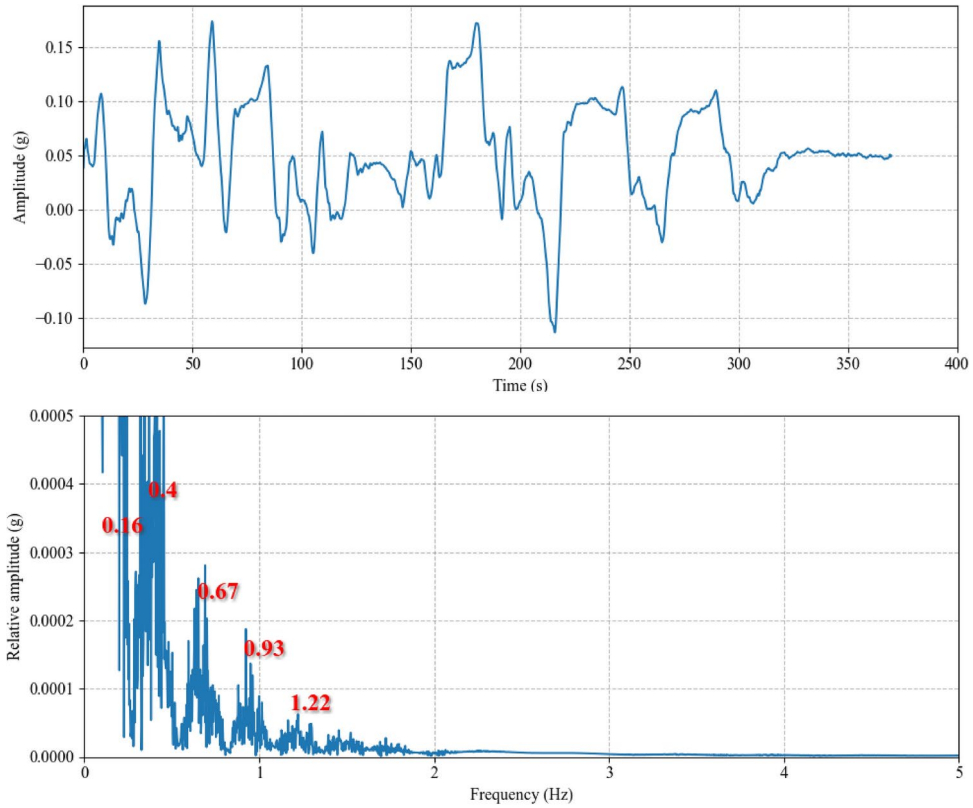

Fig. 25. Power spectrum of a bus running for the lateral acceleration of the bus seat showing dominant frequencies.

Figure 24 depicts the covariance of peak acceleration cycles for Types A and B acceleration types. As can be seen from the trend lines of covariance Type A has a slightly greater gradient, and thus plays a slightly more dominant role in increasing bus seat acceleration with respect to time compared to Type B.

Acceleration frequency

Figure 25 depicts the frequency spectrum of a bus trip showing dominant frequencies exist in the lateral acceleration. It can be seen that at lower peak frequencies the amplitude of the acceleration was higher than the higher frequencies. The relationship between frequency and amplitude was an exponential decay function. The highest longitudinal frequency was at 1.22 Hz and had approximately a relative amplitude of 0.00006 g which translated to 0.06 g as observed in the analysis. Also, all the peak frequencies namely 0.16, 0.4, 0.67, 0.93 and 1.22 Hz had different amplitudes. This indicated that the frequency of vibrations can be predicted from the

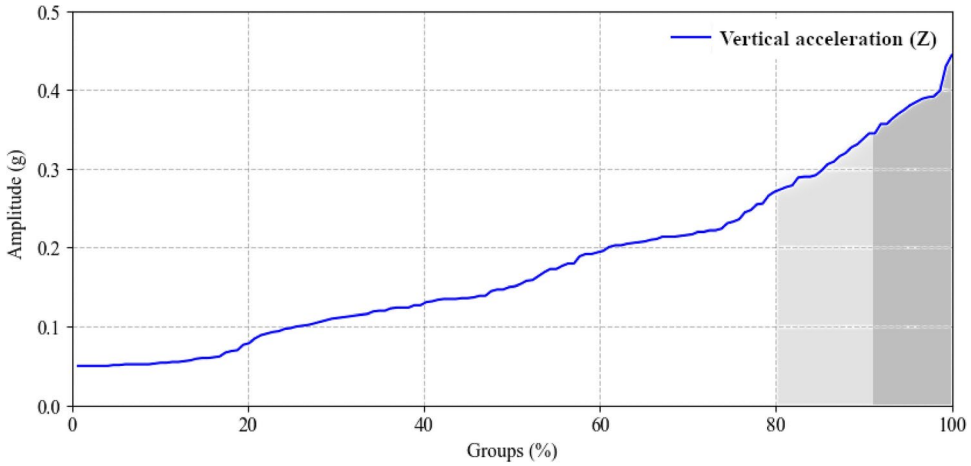

Fig. 26. Bus vertical peak acceleration cycles instances ordered from low to high amplitude.

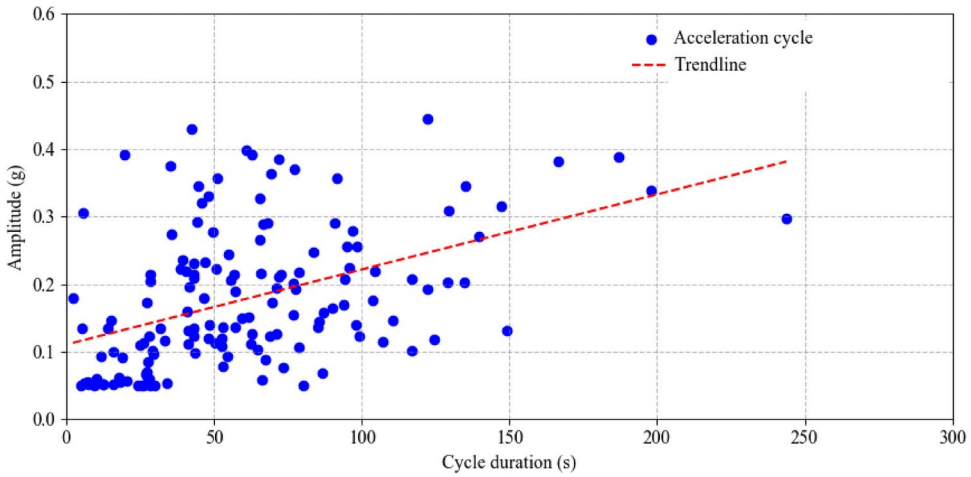

Fig. 27. Peak amplitude of bus vertical acceleration instance points versus corresponding cycle duration.

vibration amplitudes. Both the longitudinal and lateral acceleration had similarity in frequency modes as can be seen from the lateral acceleration frequency spectrum.

From the frequency spectrum, the major acceleration types can be identified. Peak frequencies namely 0.67, 0.93 and 1.22 Hz corresponded to the bus's different transient acceleration modes where 0.16 and 0.4 Hz accelerations correlated to the gradual bus acceleration modes. As the bus was mostly rigid body vibration for the seat vibration, higher frequencies than 1.2 Hz relating to loose parts vibration were not observed in the frequency spectrum.

Vertical acceleration analysis

Acceleration ranges

As can be seen from Fig. 26, 50% of the acceleration peaks have g_{max} lower than 0.151 g. This also means 50% of the acceleration peaks have g_{max} greater than 0.151 g. On the other hand, 20% of the acceleration peaks have g_{max} greater than 0.270 g (grey shade). Only 8.1% of the acceleration peaks have g_{max} greater than 0.350 g (dark grey shade).

The histogram data of peak acceleration cycles can be divided into two sections based on the gradient change at 75%. During a bus trip, either bus driving acceleration (75% of the time) or bus starting to move and stopping acceleration (25% of the time) could occur. It can be seen that the driving acceleration range was between 0.05 and 0.23 g with the median at 0.12 g. The bus starting to move and stopping acceleration range was between 0.23 g and 0.44 g with the median at 0.32 g.

Compared to the longitudinal and lateral acceleration ranges the intensity of the g_{max} acceleration range for vertical acceleration was higher during bus starting to move and stopping.

As can be seen from Fig. 27, the majority of the peak acceleration cycles fall under 73 s cycle duration where the median cycle duration for peak acceleration cycles was 53 s. The RMS acceleration of peak acceleration cycles was approximately 0.21 g.

Acceleration frequency

Figure 28 depicts the frequency spectrum of a bus trip showing dominant frequencies exist in the vertical acceleration. It can be seen that at lower peak frequencies the amplitude of the acceleration was higher than at the higher frequencies. The highest frequency at 4.5 Hz had a negligible relative amplitude. Also, all peak frequencies namely 0.10, 0.41, 0.67, 0.96, 1.2, 1.5, 1.8, 2.0, 2.6, 2.8, 3.1, 3.4, 3.7, 3.95, 4.2 and 4.5 Hz had different amplitudes. This indicated that frequencies of vibration can be predicted from vibration amplitudes. In comparison to longitudinal and lateral accelerations, vertical acceleration showed higher frequency modes as can be seen from the vertical acceleration frequency spectrum.

From the frequency spectrum, the major acceleration modes can be identified. The peak frequencies namely 0.67, 0.96 and 1.2 Hz corresponded to different transient acceleration modes where 0.10 and 0.41 Hz accelerations correlated to the gradual bus seat acceleration modes. The higher peak accelerations higher than 1.2 Hz corresponded to the bus bounce vibrations modes arising from the bus suspension system working and corresponding resonance frequencies which were captured in the frequency spectrum analysis such as frequencies including 1.5, 1.8, 2.0, 2.6, 2.8, 3.1, 3.4, 3.7, 3.95, 4.2 and 4.5 Hz. Research previously noted that the suspension system's ability to dampen vibrations absorbs frequencies between 10 and 15 Hz, with variations depending on the suspension's design and working conditions[30]. Similarly, there is an amplitude peak typically found between 2 and 3 Hz, likely due to the natural frequency of the bus's sprung mass[42].

Bus seat vibration results discussion

In summary for longitudinal acceleration, 50% of the time the acceleration was below 0.14 g, and 20% of the time it was above 0.2 g. The median acceleration during cruising was 0.12 g. Significant speed changes saw a minimum acceleration of 0.21 g, a median of 0.25 g, and a peak of 0.36 g, which was rare. The median duration for significant speed changes were 2.0, 3.2, and 6.3 seconds, while most accelerations lasted about 18 seconds. High fluctuations occurred in 20% of acceleration modes, with 5% showing no clear acceleration change. Type B acceleration, associated with stopping and starting, was more common and had a higher correlation coefficient than Type A, which caused sharper accelerations during traffic navigation. Low-frequency vibrations (0.16 to 1.2 Hz) dominated the acceleration modes, with peak cycle RMS acceleration at 0.19 g.

In summary for lateral acceleration, 50% of the acceleration modes were under 0.11 g and 20% were above 0.18 g, with a median acceleration of 0.11 g while cruising. During significant speed changes, accelerations ranged from 0.25 g to 0.42 g (the latter being rare), with median accelerations of 0.28 g. Significant speed changes lasted 2.0, 3.4, and 7.0 seconds depending on the acceleration type, while most acceleration modes lasted 24 seconds. Approximately 20% of acceleration modes experienced high fluctuations, with 5.7% showing no clear change. Type B acceleration was more prominent and associated with bus turning, stopping, and starting, while

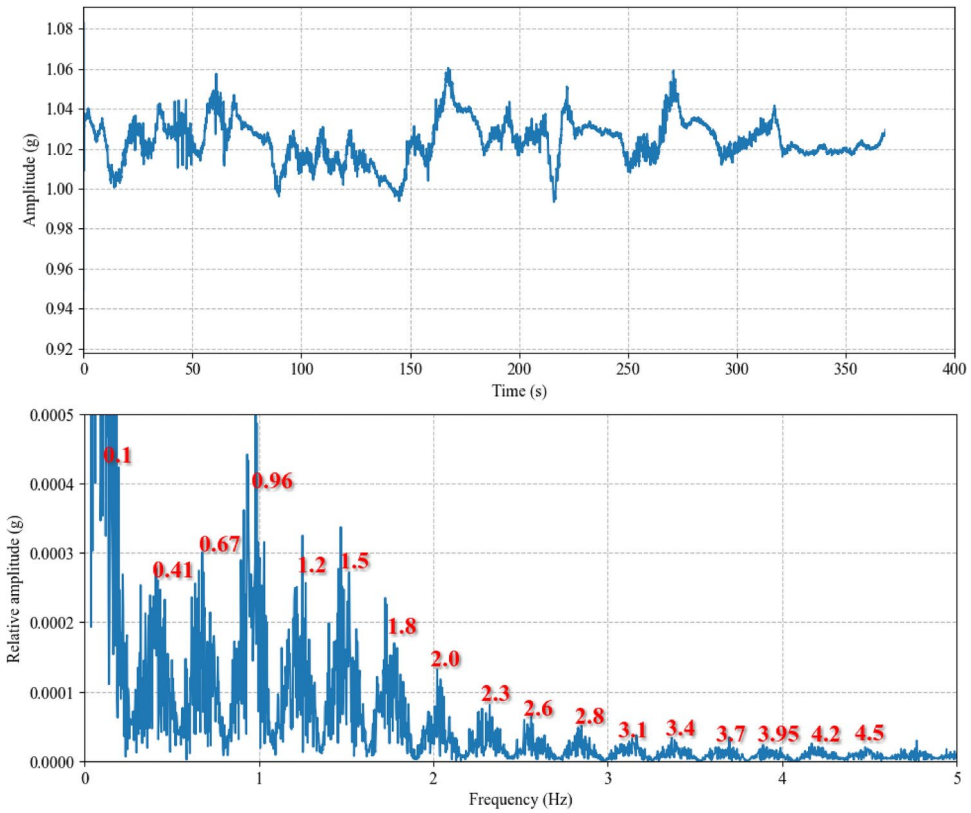

Fig. 28. Power spectrum of a bus running for the vertical acceleration of the bus seat showing dominant frequencies.

Type A acceleration was linked to sharp accelerations in traffic and on curvy roads. Low-frequency vibrations (0.16, 0.4, 0.67, 0.93, and 1.22 Hz) dominated, with RMS peak accelerations occurring at 0.16 g.

In summary for vertical acceleration, 50% of vertical accelerations were below 0.15 g, while 20% were above 0.27 g. When cruising, the median acceleration was 0.12 g. During significant speed changes, the minimum and median accelerations were 0.23 g and 0.32 g, respectively, with a peak of 0.44 g, which was rare. The median duration for significant speed changes was 53 seconds, and most acceleration modes lasted 73 seconds. Passengers experienced notable acceleration (bounce mode) during starts, stops, and jerks from road bumps and pits. As the vibration amplitude rises, acceleration becomes more pronounced, likely resulting in increased discomfort for potential passengers, with vertical acceleration being the primary factor affecting passenger comfort[20]. Low to moderate acceleration frequencies (ranging from 0.10 to 4.5 Hz) dominated the bus run, with peak acceleration modes having an RMS acceleration of 0.21 g.

Future work

The findings in this research show that city bus ride has seat vibration levels that are considerable and have implications on how the riders would perceive these vibration levels. Depending on human response to vibration levels including different age groups will shed important details of city bus ride comfort levels to different riders. The acceleration levels and comfort levels in city bus rides could be compared to other platforms in motion such as elevators. Figure 29 depicts a comparison of a bus ride versus two different elevator rides where the major acceleration modes are shown. In the bus ride, the initial steady state acceleration is bus driving acceleration followed by increasing speed acceleration (between 10 and 15 s) and finally, another rise in speed acceleration over a longer period followed by stopping. Lift acceleration A shows a smooth lift ride acceleration during the starting period of the lift from the standing still. Lift acceleration B shows a not smooth lift ride acceleration during the starting period of the lift from the standing still. It can be noticed that bus acceleration modes are higher than what is experienced during an elevator ride.

Different studies tailored for specific circumstances such as passenger comfort level to vibration exposure duration, chronic exposure consequences such as for riders who are frequent travellers, vehicle design and maintenance and driving conditions could be conducted to ensure vibration levels remain within safe limits.

Furthermore, the findings in this research could be utilised for developing advanced materials and design techniques for bus seats that can absorb and dampen vibrations more effectively. Likewise, to develop ergonomic seat designs that minimize the transmission of vibrations to the human body which can enhance passenger comfort and health. A comparative study can be conducted between different types of buses including electric, diesel, and also old vs. new models can provide insights into how design changes over time impact vibration levels and what technologies are most effective in reducing them.

Conclusions

In this paper, several techniques and approaches are presented for understanding city bus seat dynamics namely: vibration and acceleration levels in the longitudinal, lateral and vertical directions. A 6-axis IMU device is used, and peak detection algorithmic filters are applied to the accelerometer sensor data, extracting overall the city bus seat vibration acceleration performance. The results indicate the level of comfort and overall ride quality that a city bus passenger can expect, considering the various types of acceleration occurring during the bus's operation. It is shown that the median seat acceleration that occurred due to the bus running was around 0.12 g while the acceleration can be as high as 0.44 g. The high acceleration during speeding and braking of the bus introduces jerk. The perceived shaking due to jerk can be considered above light shaking and considerable due to the relatively significant g-force compared to Earth's gravitational g-force of 1 g. Jerk may be a better indicator of passenger discomfort.

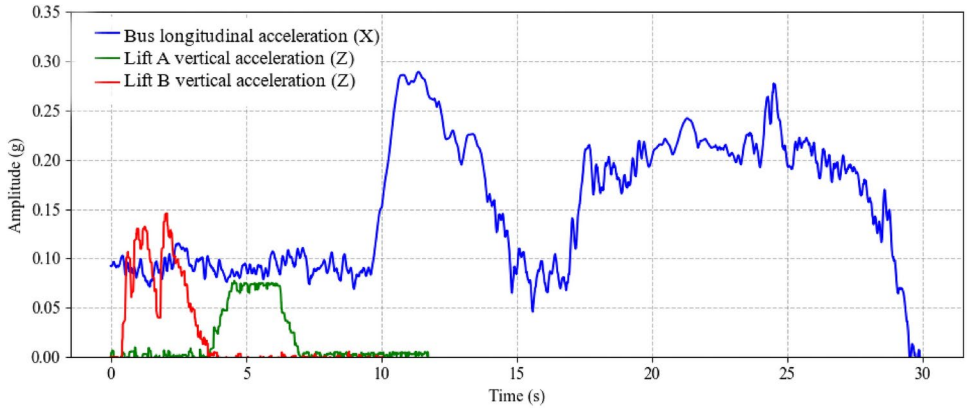

Fig. 29. Comparison of bus ride longitudinal acceleration to elevator acceleration. Smooth lift (**A**) acceleration showing gradual increase and decrease in acceleration. A not smooth lift (**B**) acceleration showing abrupt changes in acceleration.

The results presented herein can be used in future research to compare uncomfortable city bus driving conditions and also to develop an acceptable level of ride comfort for the city bus passenger. Another outcome could be the development of bus seats and suspension systems designed to improve passenger comfort by reducing the effects of starts and stops. In addition, driver behaviour data related to deceleration and acceleration can be used as a holistic approach to monitoring vehicle data, such as predictive maintenance, optimising emission reduction and reduced energy usage by the vehicle.

Data availability

The data that support the findings of this study are available from figshare repository at https://figshare.com/articles/dataset/26518570.

Received: 31 July 2024; Accepted: 21 November 2024
Published online: 02 December 2024

References

1. Lan, Y. et al. Bridge frequency identification in city bus monitoring: A coherence-PPI algorithm. *Eng. Struct.* **296**, 116913 (2023).
2. Montenegro, P. et al. Assessment of train running safety on bridges: A literature review. *Eng. Struct.* **241**, 112425 (2021).
3. Agostinacchio, M., Ciampa, D. & Olita, S. The vibrations induced by surface irregularities in road pavements-a matlab® approach. *Eur. Transp. Res. Rev.* **6**, 267–275 (2014).
4. Frej, D., Grabski, P., Jurecki, R. S. & Szumska, E. M. Experimental study on longitudinal acceleration of urban buses and coaches in different road maneuvers. *Sensors* **23**, 3125 (2023).
5. Ma, H., Xie, H., Huang, D. & Xiong, S. Effects of driving style on the fuel consumption of city buses under different road conditions and vehicle masses. *Transp. Res. Part D Transp. Environ.* **41**, 205–216 (2015).
6. He, Y., Yan, X., Wu, C., Chu, D. & Peng, L. Effects of driver's unsafe acceleration behaviors on passengers' comfort for coach buses. In *ICTIS 2013: Improving Multimodal Transportation Systems-Information, Safety, and Integration*, 1649–1655 (2013).
7. Vaiana, R. et al. Driving behavior and traffic safety: an acceleration-based safety evaluation procedure for smartphones. *Mod. Appl. Sci.* **8**, 88 (2014).
8. Hossain, M. I., Eager, D. & Walker, P. D. Greyhound racing ideal trajectory path generation for straight to bend based on jerk rate minimization. *Sci. Rep.* **10**, 7088. https://doi.org/10.1038/s41598-020-63678-1.
9. Pendrill, A.-M. Rollercoater loop shapes. *Phys. Educ.* **40**(16), 517–521 (2005).
10. Pendrill, A.-M. & Eager, D. Velocity, acceleration, jerk, snap and vibration: forces in our bodies during a roller coaster ride. *Phys. Educ.* **55**, 065012. https://doi.org/10.1088/1361-6552/aba732 (2020).
11. Förstberg, J. *Ride comfort and motion sickness in tilting trains. Human responses to motion environments in train and simulator experiments.* Ph.D. thesis, Department of Vehicle Engineering, Royal Institute of Technology, Stockholm (2002).
12. Johanning, E. Back disorders and health problems among subway train operators exposed to whole-body vibration. *Scand. J. Work Environ. Health* 414–419 (1991).
13. Boshuizen, H., Bongers, P. & Hulshof, C. Self reported back pain in fork-lift truck and freight-container tractor drivers exposed to whole-body vibration. *Spine* **17**, 59–65. https://doi.org/10.1097/00007632-199201000-00010 (1992).
14. Whyte, T., Gibson, T., Anderson, R., Eager, D. & Milthorpe, B. Mechanisms of head and neck injuries sustained by helmeted motorcyclists in fatal real-world crashes: Analysis of 47 in-depth cases. *J. Neurotrauma* **33**(19) (2016).
15. Pope, M. H., Magnusson, M. & Wilder, D. G. Low back pain and whole body vibration. *Clin. Orthop. Relat. Res.* **1976–2007**(354), 241–248 (1998).
16. Porter, J. M. & Gyi, D. The prevalence of musculoskeletal troubles among car drivers. *Occup. Med.* **52**, 4–12 (2002).
17. Nahvi, H., Fouladi, M. H. & Nor, M. M. Evaluation of whole-body vibration and ride comfort in a passenger car. *Int. J. Acoust. Vib.* **14**, 143–149 (2009).
18. Suzuki, H. Research trends on riding comfort evaluation in japan. *Proc. Inst. Mech. Eng. Part F J. Rail Rapid Transit* **212**(1), 61–72 (1998).
19. Dumitriu, M. & Stănică, D. I. Study on the evaluation methods of the vertical ride comfort of railway vehicle—mean comfort method and Sperling's method. *Appl. Sci.* **11**, 3953. https://doi.org/10.3390/app11093953 (2021).
20. Sun, R., Wang, J. & Liu, Y. Dynamic analysis and seat selection of bus driving comfort under different road conditions. *Appl. Sci.* **13**, 4639 (2023).
21. Jiang, Y., Chen, B. K. & Thompson, C. A comparison study of ride comfort indices between sperling's method and en 12299. *Int. J. Rail Transp.* **7**, 279–296 (2019).
22. Moon, S. & Yi, K. Human driving data-based design of a vehicle adaptive cruise control algorithm. *Veh. Syst. Dyn.* **46**, 661–690 (2008).
23. Bryce, W. A human criterion for the acceptance of transverse seat vibration. *J. Sound Vib.* **3**, 384–392 (1966).
24. Bhiwapurkar, M. K., Saran, V. H. & Harsha, S. P. Seat to head transmissibility during exposure to vertical seat vibration: Effects of posture and vibration magnitude. *Int. J. Acoust. Vib.* **24**, 3–11 (2019).
25. Clark, W. S., Lange, K. O. & Coermann, R. R. Deformation of the human body due to uni-directional forced sinusoidal vibration. *Hum. Factors* **4**, 255–274 (1962).
26. Chen, J. et al. Predictors of whole-body vibration levels among urban taxi drivers. *Ergonomics* **46**, 1075–1090. https://doi.org/10.1080/0014013031000109205 (2003).
27. Funakoshi, M., Taoda, K., Tsujimura, H. & Nishiyama, K. Measurement of whole-body vibration in taxi drivers. *J. Occup. Health* **46**, 119–124 (2004).
28. Zhang, G. & Ye, D. Eleven dof vehicle dynamics model and comfort simulation. *Mach. Des. Manuf.* **1**, 43–46 (2017).
29. Bogsjö, K., Podgórski, K. & Rychlik, I. Models for road surface roughness. *Veh. Syst. Dyn.* **50**, 725–747 (2012).
30. Nguyen, T., Swolana, P., Lechner, B. & Wong, Y.D. An experimental comparison of mathematical heavy-duty city bus models to evaluate passenger ride comfort induced by road roughness. *Math. Comput. Model. Dyn. Syst.* **27**, 203–221 (2021).
31. Long, L. X., Quynh, L. V. & Cuong, B. V. Study on the influence of bus suspension parameters on ride comfort. *Vibroeng. Procedia* **21**, 77–82 (2018).
32. Mazzeo, M., De Domenico, D., Quaranta, G. & Santoro, R. An efficient automatic modal identification method based on free vibration response and enhanced empirical Fourier decomposition technique. *Eng. Struct.* **298**, 117046 (2024).
33. Zini, G., Giachetti, A., Betti, M. & Bartoli, G. Vibration signature effects on damping identification of a RC bridge under ambient vibrations. *Eng. Struct.* **298**, 116934 (2024).
34. sensemore. What is envelope analysis? (2024).
35. Carr, M. Moving average envelopes: A popular trading tool (2023).
36. Beavers, I. The case of the misguided gyro.

37. Pan, C., Zhang, R., Luo, H. & Shen, H. Baseline correction of vibration acceleration signals with inconsistent initial velocity and displacement. *Adv. Mech. Eng.* **8**, 1687814016675534 (2016).
38. Eager, D., Pendrill, A.-M. & Reistad, N. Beyond velocity and acceleration: Jerk, snap and higher derivatives. *Eur. J. Phys.* **37**(6), 065008. https://doi.org/10.1088/0143-0807/37/6/065008 (2016).
39. Hayati, H., Eager, D., Pendrill, A.-M. & Alberg, H. Jerk within the context of science and engineering—A systematic review. *Vibration* **3**(4), 371–409 (2020).
40. Aroeira, C. Vibration analysis and envelope (2024).
41. Bae, I., Moon, J. & Seo, J. Toward a comfortable driving experience for a self-driving shuttle bus. *Electronics* **8**, 943 (2019).
42. Pérez, J., Olazagoitia, J., Badea, F. *et al.* Characterization of urban bus acceleration cycles for fatigue analysis with a portable low-cost acquisition system. *J. Sens.* **2022** (2022).

Author contributions
D.E. conceived the experiment(s), M.I.H. conducted the experiment(s), D.E., M.I.H, A.L.L. and S.Z. analysed the results. All authors reviewed the manuscript.

Declarations

Competing interests
The authors declare no competing interests.

Additional information
Correspondence and requests for materials should be addressed to M.I.H.

Reprints and permissions information is available at www.nature.com/reprints.

Publisher's note Springer Nature remains neutral with regard to jurisdictional claims in published maps and institutional affiliations.